AT622 Section 16
Radiative Properties of Clouds

Here we provide an overview of the properties of clouds that define how much radiation is absorbed in the atmosphere and how much radiation escapes through the boundaries of the atmosphere. The properties of relevance include:

(1) The three dimensional distribution of the cloud. This influence is usually thought of in terms of separate vertical and horizontal effects. Vertical variability is dealt with in models by introducing cloud overlap assumptions (e.g., Geleyn and Hollingworth, 1979). Horizontal variability is dealt with using assumptions involving cloud amount (Stephens, 1988). Either is empirical and a critical assessment of the uncertainties associated, with assumptions of each, is lacking. Research is now beginning to demonstrate how the 3D nature of clouds is perhaps the most significant factor determining the radiative transfer. Hereafter the macroscopic cloud properties that determine this influence are referred to as *extrinsic optical properties* (EOP). We will consider only the most basic aspects of the effects of these properties on radiation.

(2) The internal optical properties of the cloud. These properties are intrinsically defined by cloud microphysics (such as size and shape of particles). In the case of ice clouds, our understanding of the relationship between optical properties to ice particle microphysics is qualitative. Global climate models and most cloud resolving models do not predict the relevant microphysical properties even of water clouds. Most parameterizations are then carried out in terms of the predictable water or ice mass and a specified microphysical parameter (such as effective particle size). The optical properties of clouds defined by the intrinsic microphysics of clouds will hereafter be referred to as *intrinsic optical properties* (IOP). The single scatter albedo is an example of an IOP. As shown below, cloud optical depth is defined both by macroscopic properties (e.g., cloud depth) and microphysical properties (such as particle size) and thus is a combination of both.

16.1 Intrinsic IR Optical Properties—Cloud Emissivity

The effect of IOPs on IR radiative properties of clouds is generally thought to be negligible as it is commonly assumed that scattering by cloud particles at infrared wavelengths is negligibly small (despite the fact that $\tilde{\omega}_o \approx 0.5$). Some support of this assumption is given in Fig. 16.1, which suggests that the longwave reflectivity of the thickest of clouds is only a few percent. However, even a relatively small amount of scattering has effects both on the emissivity of high clouds (Stephens, 1980) and subsequently IR heating rates of these clouds (discussed below).

Ignoring at first the effects of scattering, we might deduce from Fig. 16.1 that the gray-body assumption is reasonable (i.e., the properties of reflection and absorption are spectrally flat). If we work on the assumption that absorption is dominant, then

$$\tau \approx \tau_{abs}$$

and

$$\tau_{abs} \approx kW$$

where k is an 'absorption' coefficient. We introduce the following for the cloud emissivity

$$\varepsilon = 1 - \exp(-\beta k W) \tag{16.1}$$

where β is the diffusivity ($\beta \approx 1.66$). [Note how W for clouds is entirely analogous to u for gases.]

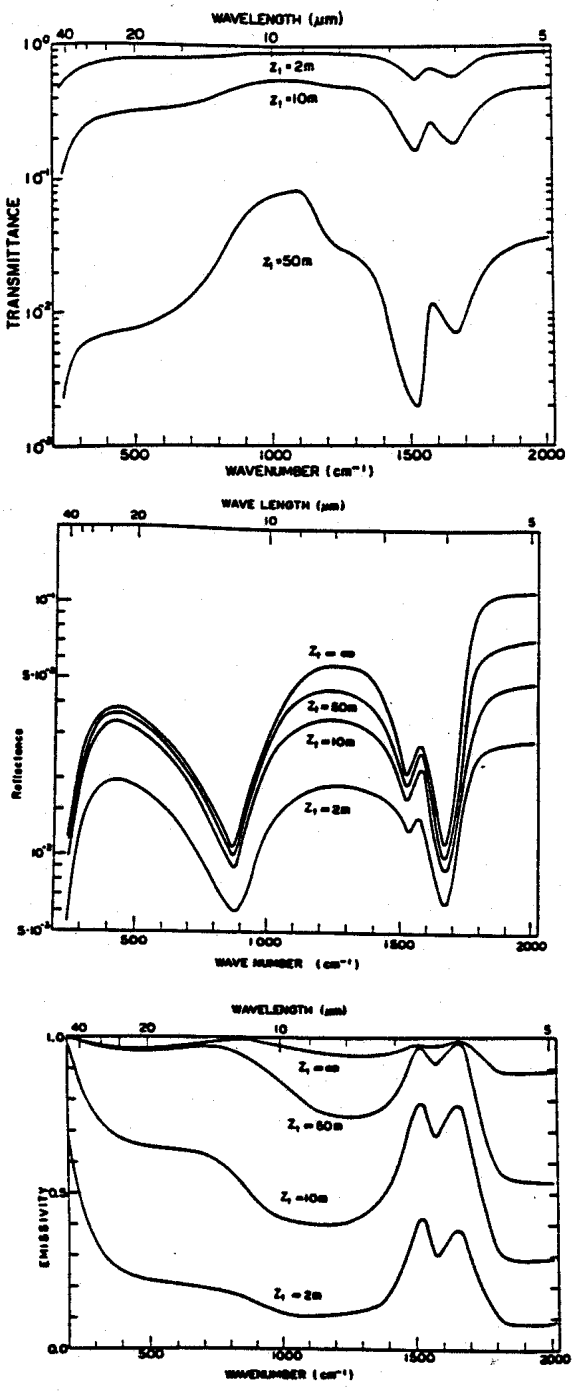

Fig. 16.1 (a) Spectral transmittance of a cloud of various thickness. Altostratus cloud with a liquid water content of 0.28 gm^{-3} (Yamamoto et al., 1970). (b) Spectral reflectance of a cloud. Same characteristics as (a) (Yamamoto et al., 1970). (c) Spectral emissivity of a cloud. Same characteristics as (a) (Yamamoto et al., 1970).

In this context, k is an inherent optical property and it is derived, or estimated, in the following way. Consider the emissivity form of flux equations

$$F^{\uparrow}(z) = F^{\uparrow}(z_b)(1-\varepsilon^{\uparrow}) + \varepsilon^{\uparrow}\sigma T_c^4$$
$$F^{\downarrow}(z) = F^{\downarrow}(z_t)(1-\varepsilon^{\downarrow}) + \varepsilon^{\downarrow}\sigma T_c^4 \qquad (16.2)$$

applicable to a single cloud layer from which

$$\varepsilon^{\uparrow}(z) = \frac{F^{\uparrow}(z_b) - F^{\uparrow}(z)}{F^{\uparrow}(z_b) - \sigma T_c^4}$$
$$\varepsilon^{\downarrow}(z) = \frac{F^{\downarrow}(z_t) - F^{\downarrow}(z)}{F^{\downarrow}(z_t) - \sigma T_c^4} \qquad (16.3)$$

follows as an inversion. Observations of $F^{\uparrow,\downarrow}$, T_c (as best estimated) and W are used to derive $\varepsilon^{\uparrow,\downarrow}$ and hence $k^{\uparrow,\downarrow}$ from Eqn. (16.3). Table 16.1 summarizes various estimates of k published in the literature. Figures 16.2a,b show examples of longwave intensities and fluxes obtained from aircraft measurements in clouds and shows how Eqn. (16.3) fits these data. Figure 16.2c shows this relationship fitted against model simulations of broadband longwave fluxes.

Table. 16.1 Summary of the cloud mass absorption coefficients [mainly ($k^{\uparrow,\downarrow}$)] in m^2g^{-1} for low-level water cloud and upper level cirrus cloud

βk^c	Source	Type of measurement
Boundary layer cloud		
0.13-0.16	Stephens (1978)	Theoretical
0.13	Platt (1976)	Vertical narrowband (10-12 μm) radiance
0.11-0.15	Schmetz, et al. (1981)	Vertical narrowband (11 μm) radiance
0.13	Bonnel, et al. (1980)	Vertical narrowband (8-14 μm) radiance
0.08	Stephens, et al. (1978)	Broadband hemispheric irradiance
Cirrus cloud		
0.08	Paltridge and Platt (1981)	Vertical narrowband (10-12 μm) radiance
0.056	Ibid	Broadband hemispheric irradiance
0.076-0.096	Griffith, et al. (1980)	Broadband hemispheric irradiance

Given a simple expression for cloud emissivity and the profile of cloud liquid (or ice) water content, it is a simple matter to derive the longwave flux profiles through a cloud layer using Eqn. (16.2). Examples of this kind of calculation are presented in Fig. 16.3a for $F^{\uparrow,\downarrow}$ at 10 μm and in Figs. 16.3b,c for F_{net}. The downward fluxes increase rapidly from cloud top (depending on the growth of ε) and the upward flux, which at cloud base exceeds the black body flux, decreases into the cloud. Both $F^{\downarrow}$ and $F^{\uparrow}$ approach the equivalent black body fluxes at the respective cloud boundaries where $\varepsilon^{\uparrow,\downarrow} \approx 1$.

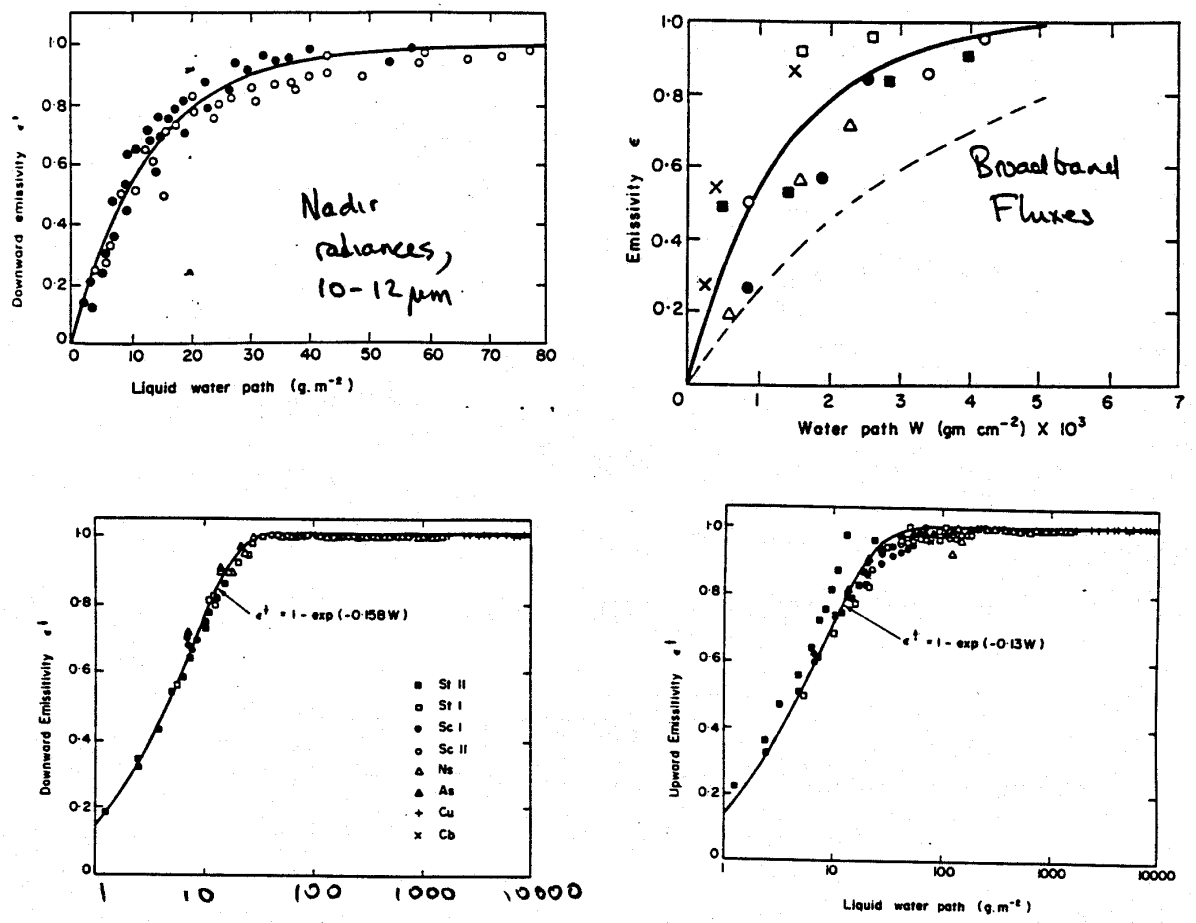

Fig. 16.2 Experimental values of 10-12 μm emissivity determined from nadir radiance measurements as a function of liquid water path. The solid and open points are the measured values. (b) Mean cloud emissivity versus total water path W to cloud top. (c) Empirical presentation of downward (a) and upward (b) emissivity as a function of liquid water path. The solid line is the least-squares best fit through the given points using the analytic form described in the text.

The net flux profiles presented in Figs. 16.3b,c show how the changing $F^{\downarrow}$ at cloud top influences F_{net} there and how the changing $F^{\uparrow}$ at cloud base governs the profile of the F_{net} in the lower portions of the cloud. The contribution of both depends on the optical thickness (Fig. 16.3b) and the temperature difference between cloud and ground (Fig. 16.3c). These dependencies vary with wavelength. The results shown in Fig. 16.3 apply to a cloud overlying a surface with no atmosphere above or below it. Figures 16.4a,b presents longwave flux profiles actually observed in clouds and features similar to those illustrated in Fig. 16.3 and are easily recognized.

16.2 Intrinsic Solar Optical Properties

The influence of cloud IOP on solar radiative transfer is complex and germane to a number of current cloud-radiation issues thought to be important to topics of climate and global change (e.g., the so-called Twomey effect).

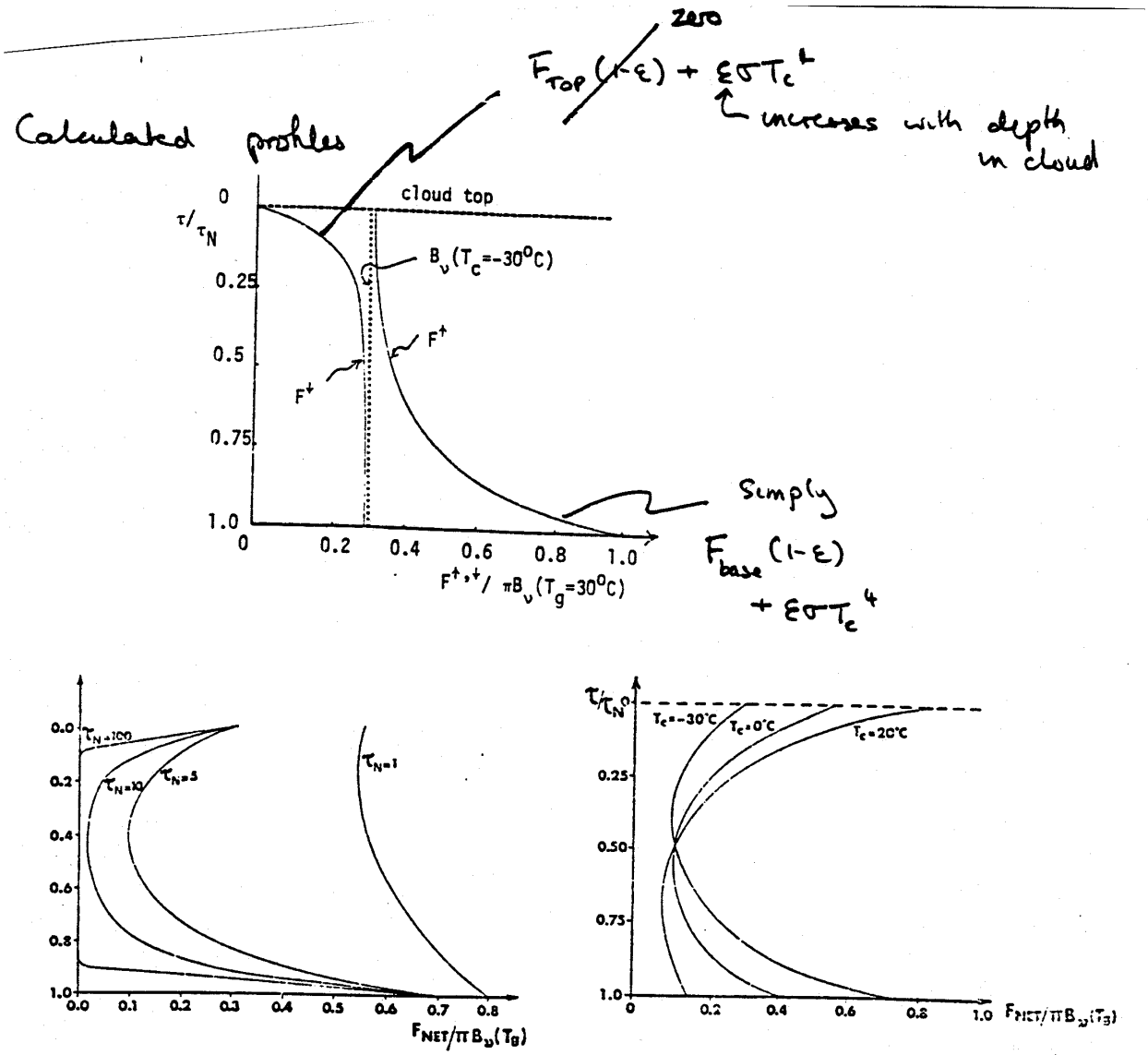

Fig. 16.3 (a) The 10 μm flux profiles for an Sc cloud layer of optical thickness $\tau_N = 5$. (b) The 10 μm net flux profiles as a function of optical thickness, $T_g = 30°$. (c) The 10 μm net flux profiles for an Sc cloud layer possessing three different cloud temperatures, $T_g = 30°C$ and $\tau_N = 5$.

The relation between IOPs and solar transfer may be explored in the context of our simple two stream model solutions in the limit as $\tau^* \to 0$ and $\tau^* \to \infty$. For optically thick, we deduce from Eqn. (15.22) that the albedo (and hence absorption) depends as follows

$$R_\infty = R(\tilde{\omega}_o, b(g), D, \mu_o) \tag{16.4a}$$

$$A_\infty = 1 - R_\infty \tag{16.4b}$$

where R_∞ and A_∞ are respectively the albedo and absorption of this 'semi-infinite' cloud. According to these simple relationships both the albedo and absorption approach fixed asymptotic limits as τ^* increases. It is relatively straightforward to show that these limits may largely be considered to depend on $\tilde{\omega}_o$ using Eqns. (15.22) and (15.21) as a guide. Stephens and Tsay showed that

$$A_\infty \approx \text{constant} \times (1-\tilde{\omega}_o)^{0.4} \tag{16.5}$$

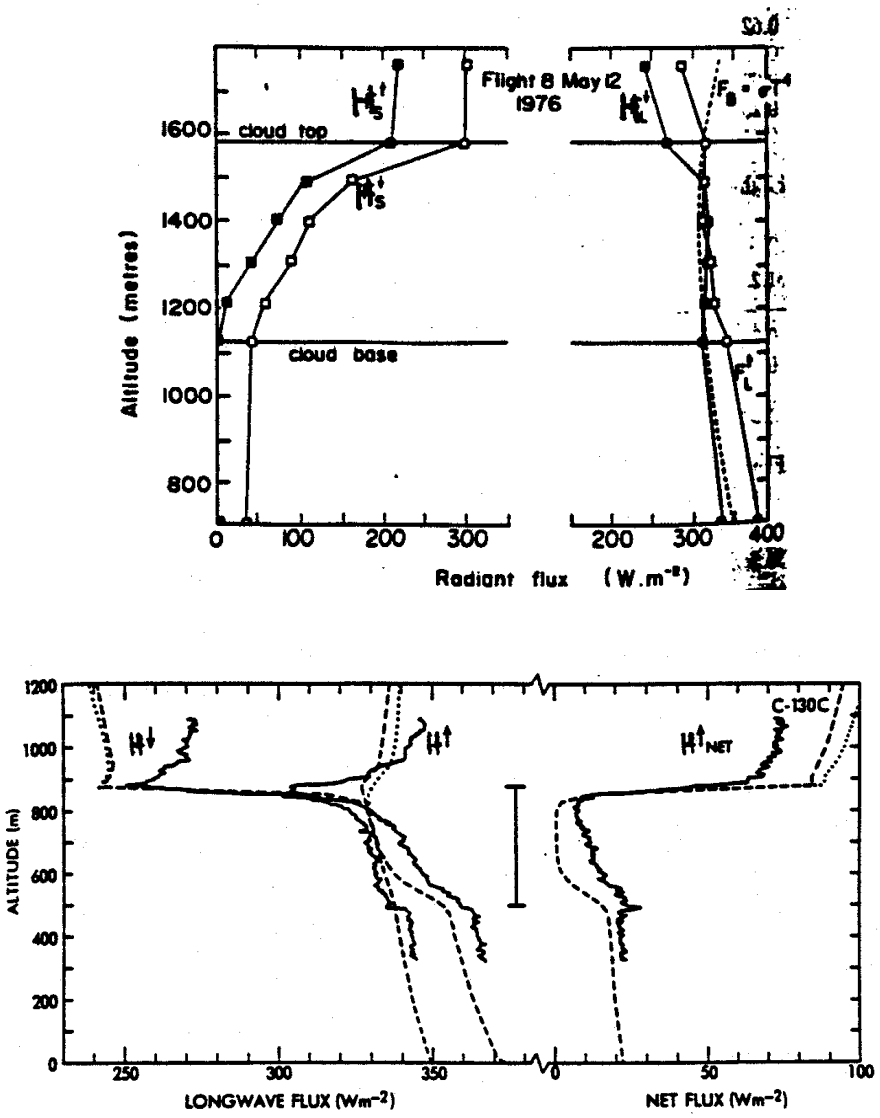

*Fig. 16.4 The total longwave and shortwave flux profiles measured in three Sc cloud layers $F_s^{\uparrow,\downarrow}$, $F_L^{\uparrow,\downarrow}$ and F_B are the shortwave and longwave fluxes, and black body flux, respectively. Each point is a 4 min average value. (b) Comparison of the observed upward $F^{\uparrow}$, downward $F_{\downarrow}$ and the net F_{net} longwave fluxes measured by the C-130 on profile C with the theoretical fluxes from the radiation scheme of Schmetz and Raschke (1981), shown as the dashed lines. The fluxes from the scheme of Roach and Slingo (1979) are within about 2 Wm^{-2} of these values, except above the cloud top where they are shown by the dotted lines. Slingo et al, 1982: QJRMS, **108**, 833-838.*

For optically thin clouds with $\tau^* \to 0$, it can also be shown (e.g., from Eqn. (15.22) and Stephens and Tsay, 1990)

$$R_o = \frac{\tau^*}{\mu_o}\tilde{\omega}_o b_o \tag{16.6.a}$$

$$T_o = 1 - \frac{\tau^*}{\mu_o}(1 - \tilde{\omega}_o f_o) \tag{16.6b}$$

and

$$A_o = \frac{\tau^*}{\mu_o}(1 - \tilde{\omega}_o) \tag{16.6c}$$

Thus both the albedo and absorption of thin clouds vary linearly with optical thickness and, as expected, respectively depend on the backscatter and absorption properties of the individual cloud particles.

These relations provide us with a way of deducing the effects of particle size on the albedo and absorption of solar radiation. Two factors that are important are:

- The first is a reciprocal dependence of optical depth on particle size

$$\tau = \frac{3W}{2\rho_{water} r_e} \tag{16.7a}$$

  where W is the liquid water path (LWP), r_e is the effective radius (the ratio of volume to area of the distribution) and ρ_{water} is the density of water. The same sort of reciprocal relationship follows for ice clouds (e.g., Fu and Liou, 1993). An alternative relation is

$$\tau = 2\pi h N_o^{1/3} \ell^{2/3} \tag{16.7b}$$

  where h is the cloud thickness, N_o is the number density of particles and ℓ is the liquid water content ($W \approx \ell h$). Both relationships predict that for fixed liquid water content or path, the optical depth increases through increases in N_o or equivalently through decreases in r_e. Such an increase in optical depth implies increased albedo of clouds through Eqn. (16.6a) but not necessarily an increase in the albedo of thick clouds since the reflection of these clouds is largely insensitive to any changes in optical depth if deep enough.

- The second factor involves the relationship between $1 - \tilde{\omega}_o$ and r_e, which Ackerman and Stephens (1987) simplify to

$$1 - \tilde{\omega}_o \approx \text{constant} \times \kappa r_e^p \tag{16.8}$$

  where κ is the bulk absorption by water and $p \leq 1$.

From the relationships in Eqns. (16.7a) and (16.8), and the expressions for albedo in Eqns. (16.6a), (16.4b), and (16.5), it follows that the albedo of clouds increases as particle size decreases (Fig. 16.5a) through a combination of both decreasing in absorption (predicted from Eqn. (16.8)) and associated increases of optical depth, Eqn. (16.7a). The relationship between absorption and particle size as

highlighted in Fig. 16.5b is complex. The dependence on particle size is such that the absorption of thin clouds (i.e., small LWP) actually increases with decreasing particle size, while the reverse applies for thick clouds (or large LWP). This thick cloud dependence has been mistakenly interpreted to imply that indiscriminant increases of particle size enhances absorption in clouds explains discrepancies with observations. Marine boundary layer clouds typified by intermediate values of LWP (and optical depth) are characterized by a weak dependence on r_e.

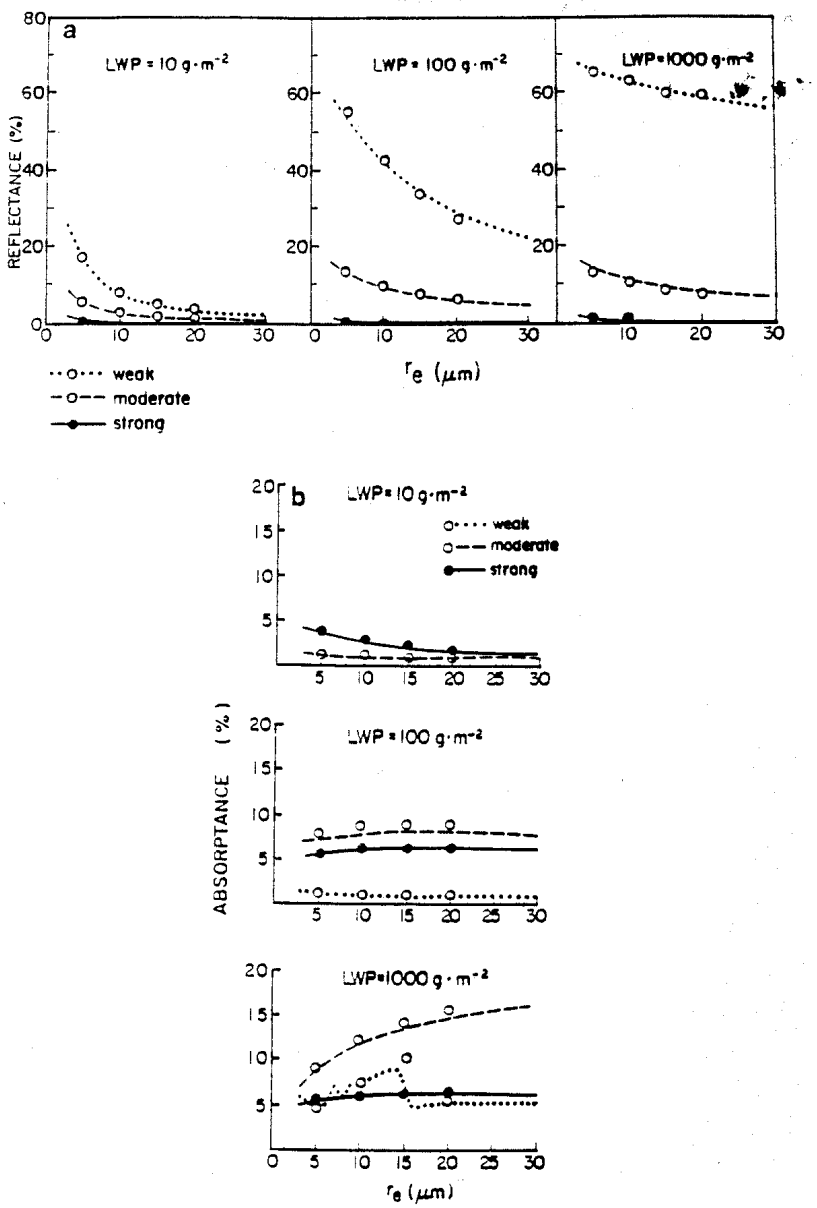

Fig. 16.5 Contributions to the (a) albedo and (b) absorptance by the three spectral absorption regimes introduced by Ackerman and Stephens (1987) as a function of r_e for specified values of LWP. The symbols refer to calculations using scattering properties from Lorenz-Mie theory (ignore differences between symbols and curves).

In summary, we deduce that the albedo of clouds is sensitive to both particle size and LWP (or IWP) and varies in a systematic way with changes in these parameters. By contrast, the solar absorption depends on these parameters in a complex way.

A series of aircraft experiments that seek to confirm the relation between r_e and cloud albedo are those of the Southern Ocean Cloud Experiments (SOCEX) described by Boers et al. (1995). They find significant seasonal variations in r_e characteristic of marine layered cloud between summer and winter (Fig. 16.6a) with composite mean values of r_e = 19 μm in winter and r_e = 13 μm in summer. Since these measurements were carried out in baseline air (free of continental effects), these results are consistent with the seasonal variations of DMS and the subsequent influence of DMS on CCNs and thus cloud microphysics. These large measured seasonal changes in r_e translate to significant percentage changes in cloud albedo (refer to Fig. 16.5a). In Fig. 16.6b the profile of effect radius is shown when the measured drizzle component is added to the measured profiles of Fig. 16.6a. This drizzle contributes significantly to the particle size at cloud base but its direct effect on the albedo of clouds has not yet been determined. The indirect effects of drizzle on albedo, through its effect on cloud evolution, are thought to be significant (Stephens, 1994).

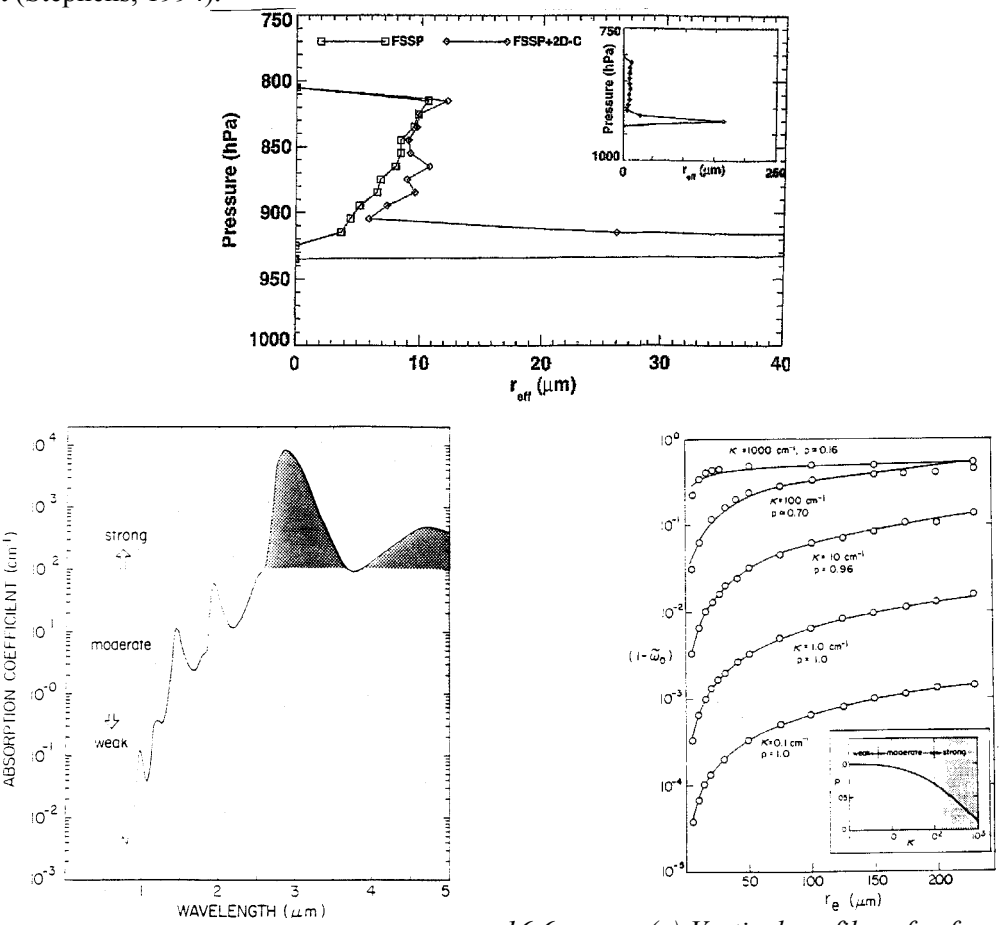

Fig. 16.6 (a) Vertical profiles of r_e from aircraft measurements of c
effective radius for selected values of ?? The solid curves represent the relationship described by Eqn. (??) for the values of p indicated and the open circles apply to the MADT theory. The insert depicts the breakdown of the weak, moderate, and strong absorption regimes.

16.3 Extrinsic Cloud Optical Properties

The most dominant control on the infrared radiative transfer through clouds is the contrast between radiation emitted from the atmosphere to the cloud from above and below and the radiation emitted from the cloud. This influence is visible in the results shown in Figs. 16.2 and 16.3. Unlike for the clear sky, the net LW radiative energy budget is largely dominated by those spectral regions that are most

transparent to gas absorption—that is in the atmospheric window. The net LW budget of a cloud is one of a balance between emission from top (cooling) and absorption from the large flux below the cloud (warming). This balance changes sign as the altitude of the cloud layer changes—net warming by high cirrus in a tropical environment is expected, net cooling for lower cloud. This variation is evident in Fig. 16.8, which shows the net longwave radiation budget of a 1 km blackbody cloud located at different levels in a standard atmosphere. This budget is defined as

$$\Delta F = F_{net}\,(\text{base}) - F_{net}\,(\text{top})$$

and this budget is more to be positive. Examples of the spectral disposition of ΔH for cirrus clouds of different thicknesses located in the tropical atmosphere and in the subarctic winter atmosphere are shown in Fig. 16.7.

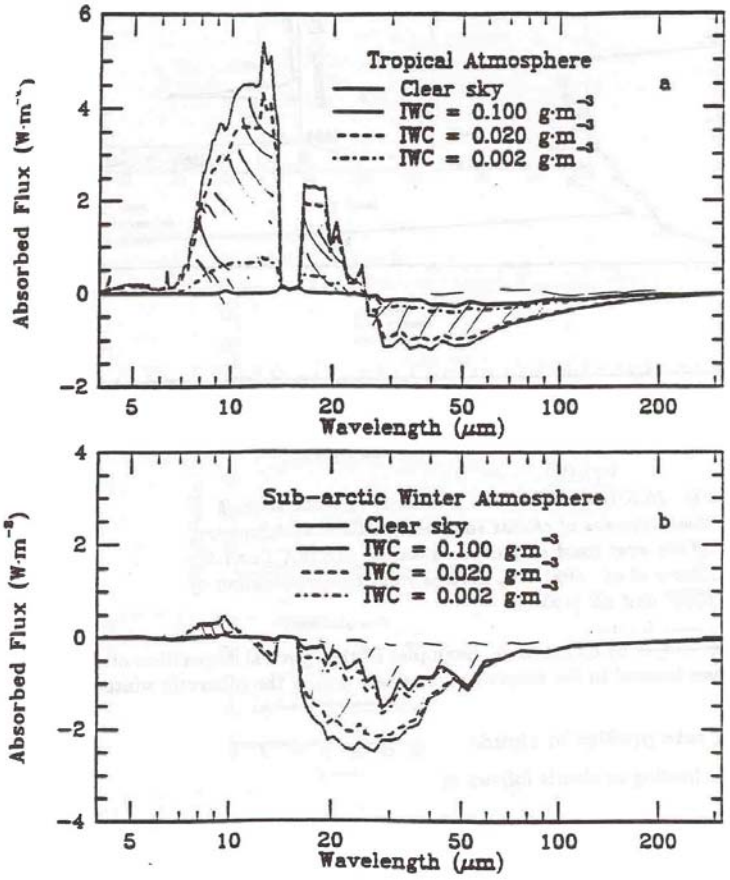

Fig. 16.7 Spectral distribution of ΔF for various cirrus clouds in (a) a tropical atmosphere and (b) a subarctic winter atmosphere.

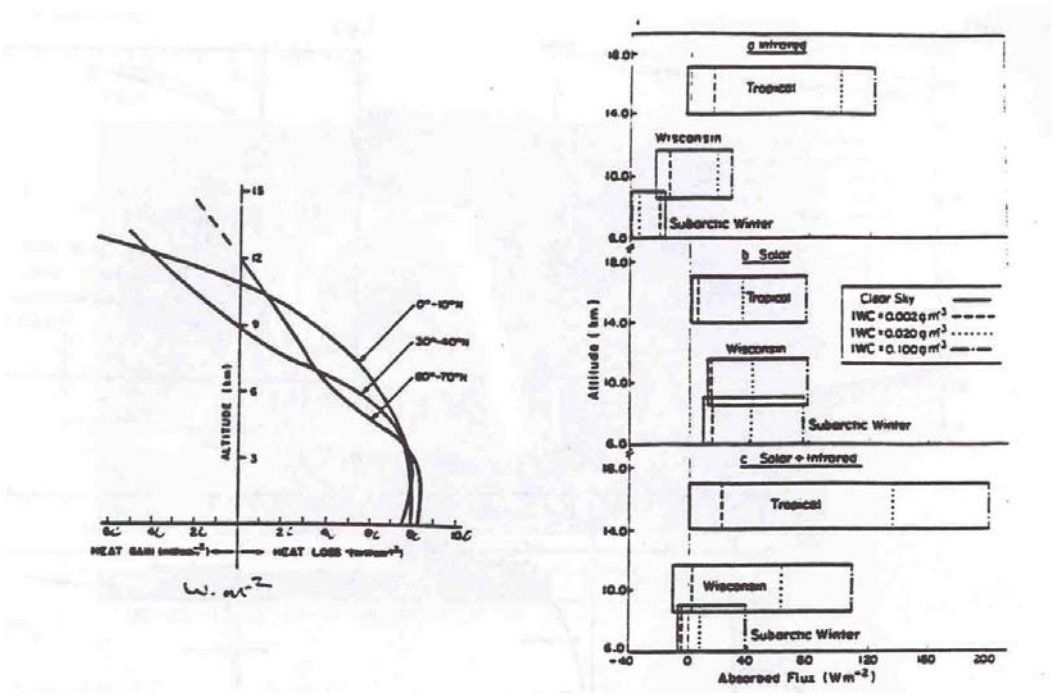

Fig. 16.8 Net radiative loss from a thin "black" cloud inserted at various heights in the mean atmospheres of three latitude zones. (After Paltridge, 1974d)

16.4 Heating Rate Profiles in Clouds

The radiative heating in clouds follows as

$$\frac{dT}{dt} = -\frac{1}{\rho C_p}\frac{dF_{net}}{dz}$$

and depends on the optical depth, cloud temperature, wavelength and all parameters that affect the fluxes (we get some sense of the effect of particle size from the above discussion). Examples of the longwave heating are given in Figs. 16.9a,b. Figure 16.9c presents the first measured profiles of solar heating and IR cooling. Generally, these profiles are characterized by radiative cooling at cloud top and warming at cloud base, although the latter is strongly dependent on the temperature differential of the radiation incident from below and the cloud temperature.

The spectral infrared heating of a cloud located in a tropical and subarctic winter atmosphere, respectively, is given in Fig. 16.10. High tropical clouds predominantly heat because the difference between emission at cloud base and absorption of radiation from below leads to a gain in radiative energy and thus a heating of high tropical clouds. This heating occurs principally in the more transparent regions of the spectrum where these differences are largest. The details of this heating and how it penetrates into the cloud also depend on the optical depth of the cloud, which under the Rayleigh assumptions, depends on the ice water path. For the lower cloud in the subarctic atmosphere, the lack of a distinct contrast between the emission from cloud base and the upwelling radiation from below leads to a much reduced heating at cloud base. These lower clouds predominantly cool at cloud top at most wavelengths.

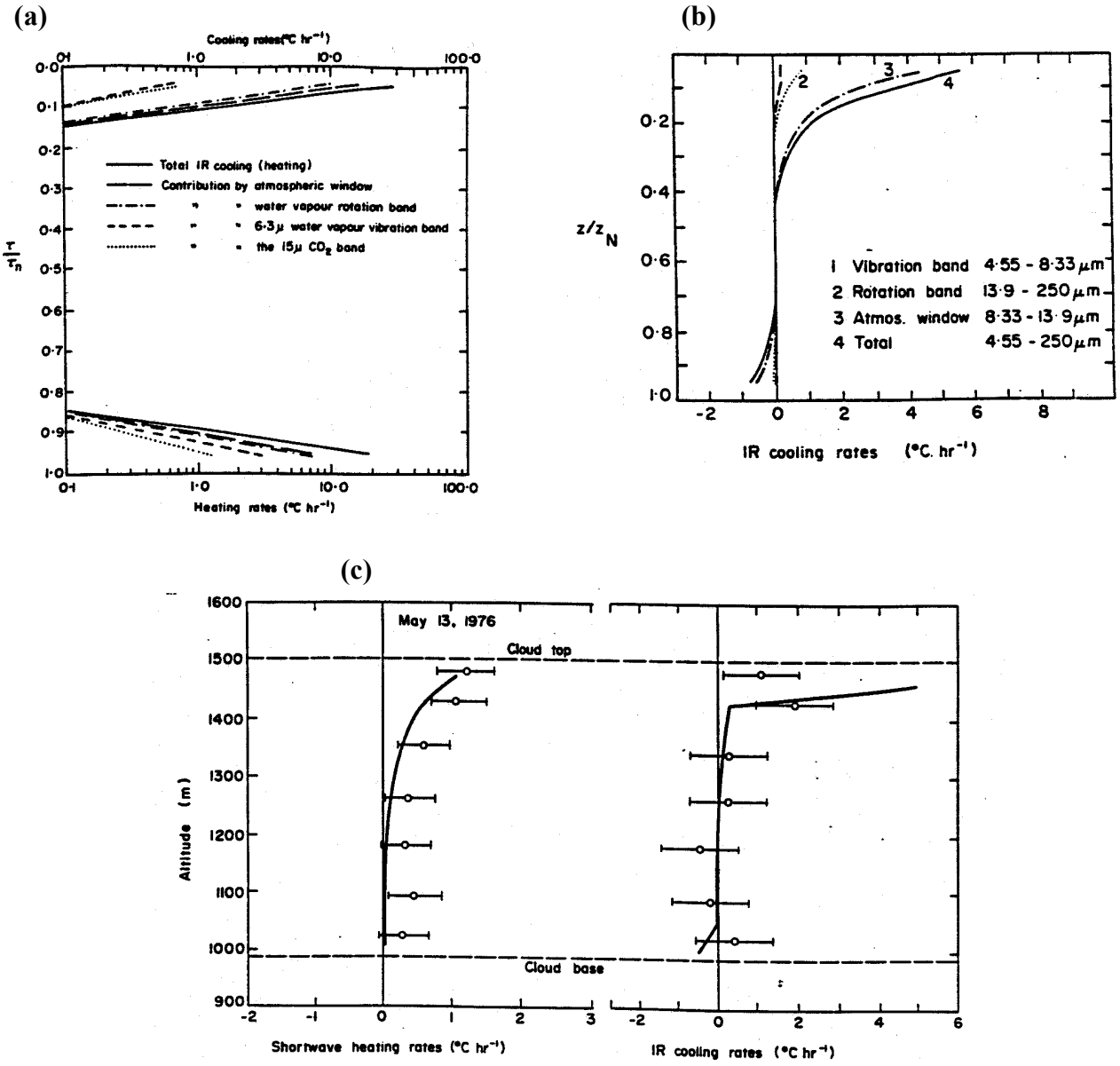

Fig. 16.9 (a) Cooling profiles for various spectral regions through an isotropic cloud at approximately 4 km altitude for a standard atmosphere with surface temepature equal to 22°C. Cloud thickenss = 1.6 km, extinction coefficient (10 μm) = 27 km^{-1}, $\tilde{\omega}_o$(10 μm) = 0.57. (b) The IR cooling rate profile in a SC I cloud layer 500 m thick positioned at 1.5 km in the tropical atmosphere model. The contributions by the three main spectral regions are displayed. (c) The shortwave and longwave heating and cooling rate profiles measured in the cloud layer sampled on 13 May 1976. The extent of the rms experimatnal error is shown by the horizontal lines. The solid curve is the theoretically calculated profile.

The important point to be drawn from this diagram is that the IR radiative properties of clouds, specifically the extent and magnitude of IR heating, is strongly dependent on the properties of the environment around the cloud (such as the temperature contrast and the amount of water vapor above and below the cloud). What is not emphasized in these diagrams but is of equal importance is the effect of optical depth (or IWP) on the radiative heating of the cloud.

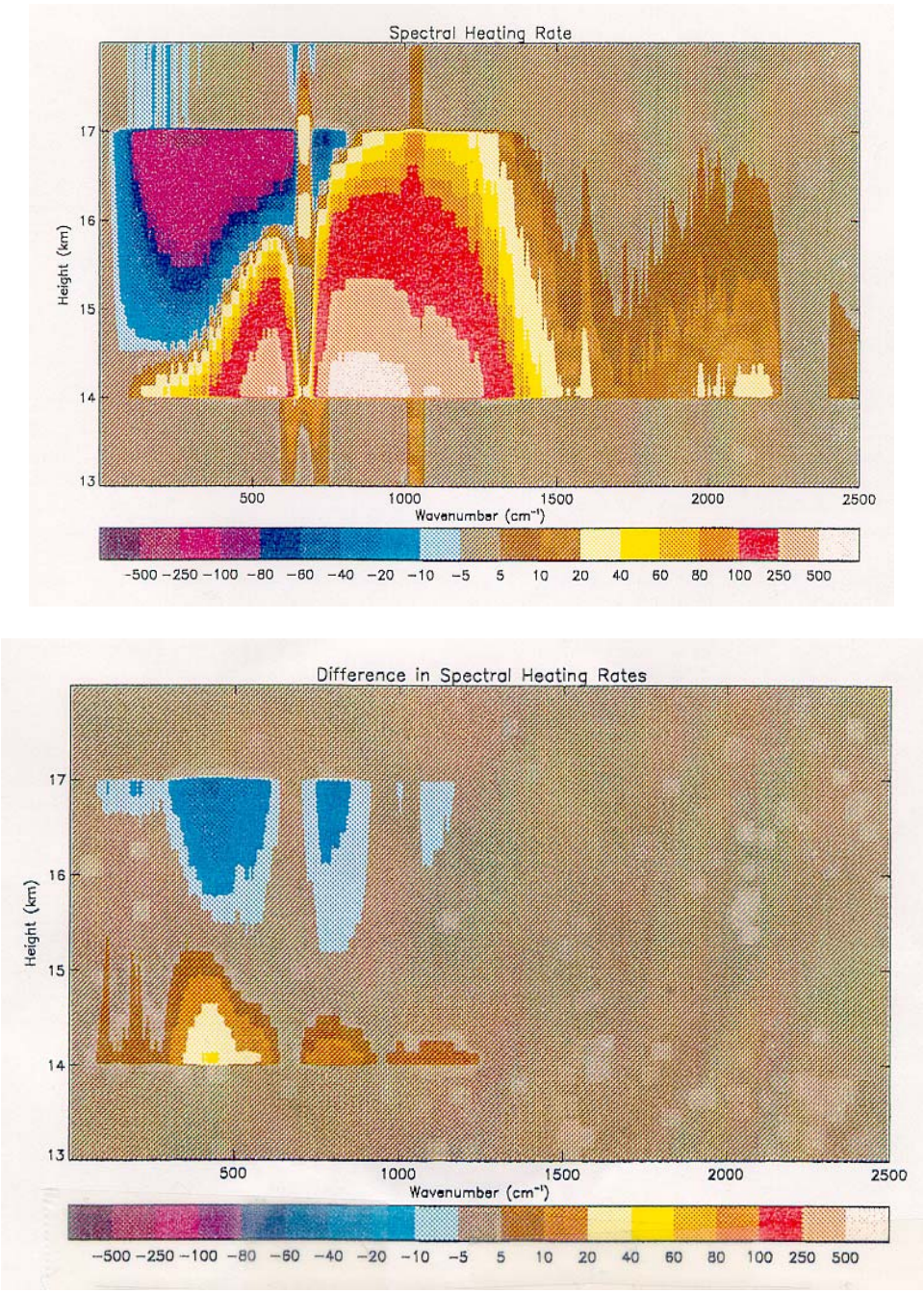

Fig. 16.10 The vertical profile of the spectral IR cooling rate for (a) an ice cloud located in a model tropical atmosphere and (b) for the same in a subarctic winter atmosphere (Edwards and Slingo, 1995).